Fullerene-Dependent Miscibility in the Silole-Containing Copolymer PSBTBT-08

Brian A. Collins,*[,†] Zhe Li,[‡] Christopher R. McNeill,[§] and Harald Ade[†]
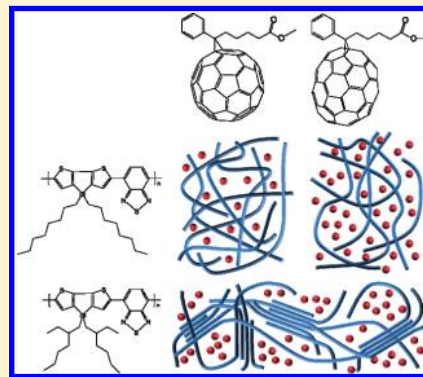
[†]Department of Physics, North Carolina State University, Raleigh, North Carolina 27695, United States
[‡]Cavendish Laboratory, University of Cambridge, J J Thomson Avenue, Cambridge CB3 0HE, U.K.
[§]Department of Materials Engineering, Monash University, Clayton, Victoria 3800, Australia

Ⓢ *Supporting Information*

ABSTRACT: A high fullerene molecular miscibility of over 40 wt % is found in the copolymer poly((4,4-octyldithieno(3,2-*b*:2′,3′-*d*)silole)-2,6-diyl-*alt*-(2,1,3-benzothiadiazole)-4,7-diyl) (PSBTBT-08)—a member of the PSBTBT low-bandgap polymer family that have produced power conversion efficiencies as high as 5.9% in solar cells. This observation suggests molecular miscibility plays a key role in the photovoltaic effect in this system. The level of miscibility is additionally measured to be highly dependent on the fullerene species with significant differences between C_{60}- and C_{70}-based fullerenes, highlighting a new parameter to be monitored and controlled when considering different fullerene moieties and species in organic solar cells. Surprisingly, a wide-angle X-ray scattering study reveals no significant crystallinity in the PSBTBT with octyl side chains, potentially the cause of low mobilities and in stark contrast to dodecyl and ethylhexyl PSBTBTs, which demonstrates the importance of the side chain in device morphology and performance.

Research into organic photovoltaic devices (OPVs) based on polymer—fullerene blends has accelerated in recent years as the physical mechanisms behind the devices are better understood and the materials used become more capable and numerous.[1] In these devices, charge generation proceeds through the dissociation of excitons at polymer/fullerene interfaces via electron transfer from polymer to fullerene or hole transfer from fullerene to polymer.[2] The exact nature of the morphology is thought to be important in determining device efficiency, with intimate mixing of polymer and fullerene maximizing exciton dissociation and interpenetrating phases facilitating charge extraction. The nature of donor—acceptor interfaces is also important, with well-defined interfaces (and interfacial dipoles) thought to assist the separation of geminate electron—hole pairs from the interface.[3,4] Pure phases are also regarded as being beneficial for device operation, minimizing the chance of charge recombination as charges are being transported to the electrodes.[5] This perspective resulted in a morphological picture of the ideal device as consisting of pure donor and acceptor phases with well-defined interfaces.[6] The efficient operation of polymer/fullerene devices has led to this paradigm being adopted by many as the working model for morphology in these systems. Recently, however, this paradigm of discrete boundaries between pure phases was challenged with the observation of a binodal in P3HT:PCBM annealed blends[7] and subsequently the explicit measurement of a substantial miscibility of [6,6]-phenyl-C_{61}-butyric acid methyl ester ($PC_{61}BM$) in poly(3-hexylthiophene) (P3HT)[7−13] and poly-(2-methoxy-5-(3′-7′-dimethyloctyloxy)-1,4-phenylenevinylene)

(MDMO-PPV).[8] Both polymers were revealed to have no pure amorphous phases when blended with $PC_{61}BM$, confounding the concept of well-defined interfaces between—and transport channels throughout—the two active components in a device. Related work involving ordered phases demonstrated intercalation of $PC_{71}BM$ in poly(2,5-bis(3-hexadecylthiophen-2-yl)thieno[3,2-*b*]thiophene (pBTTT) crystals.[14] As the range of high-performance materials continually expands through synthesis efforts,[15−18] it is important to understand how common the phenomenon of miscibility in polymer—fullerene systems really is beyond model systems and what role it plays in device function.

In this work, we show that the two most commonly used fullerenes in OPVs are both highly miscible in the dithienosilole—benzothiadiazole copolymer poly((4,4-octyldithieno(3,2-*b*:2′,3′-*d*)-silole)-2,6-diyl-*alt*-(2,1,3-benzothiadiazole)-4,7-diyl) (PSBTBT-08). Each chemical structure is displayed in Figure 1 with the fullerenes utilized being [6,6]-phenyl-C_{61}-butyric acid methyl ester ($PC_{61}BM$) and [6,6]-phenyl-C_{71}-butyric acid methyl ester ($PC_{71}BM$). The family of PSBTBT polymers has been of extensive interest due to their ability to absorb a larger portion of the solar spectrum than P3HT, thus contributing to higher power conversion efficiency.[17−21] We find that the C_{70}-based fullerene is significantly more miscible than the C_{60} derivative, demonstrating that the choice of fullerene species will have a large impact on the final
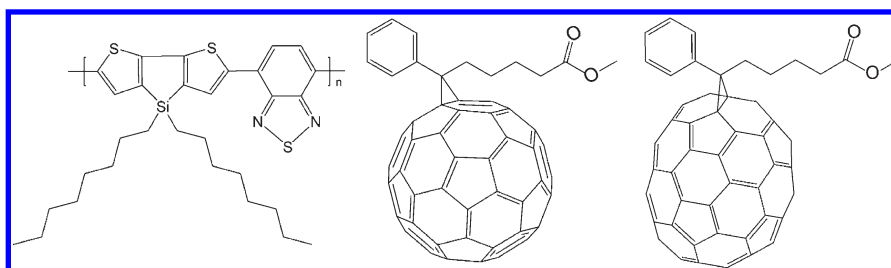
Figure 1. Chemical structures for, from right to left, PSBTBT-08, PC$_{61}$BM, and PC$_{71}$BM.
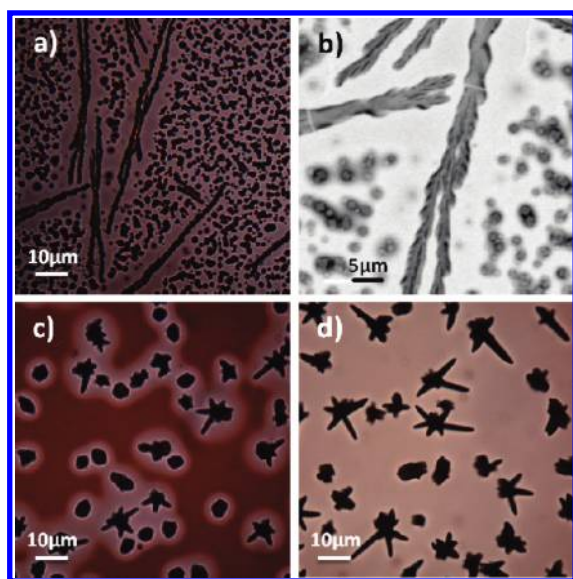

Figure 2. Images of phase-separated blends. (a and b) Transmission VLM and STXM images, respectively, of a 1:3 (w/w) PSBTBT:PC$_{61}$BM blend film annealed at 140 °C for 25 h. STXM image (transmitted intensity) acquired at 280 eV—below the carbon absorption edge where the absorption from PSBTBT heteroatoms highlight the cube-like PC$_{61}$BM crystal edges due to film thickening near the crystals. By virtue of their thickness, the PC$_{61}$BM crystals remain darker than the nominal surrounding film and appear gray, whereas PC$_{61}$BM-depleted regions are white. (c and d) Transmission VLM images of 1:3 (w/w) PSBTBT: PC$_{71}$BM at 140 °C for 25 and 116 h, respectively.

nanocomposition in OPVs. Combined with our earlier results,[7,8] fullerene miscibility is now confirmed with two fullerenes in three polymers, suggesting that polymer—fullerene miscibility is a general phenomenon that must be accounted for in describing device morphology and understanding device function.

The present measurements employed the same methods used in the previous studies, namely quantitative fitting of near-edge X-ray absorption fine structure (NEXAFS) spectra acquired in fullerene-depleted regions of blend films brought to thermodynamic equilibrium.[8] To understand the potential effect of polymer crystallization on the measurement of miscibility, grazing incidence wide-angle X-ray scattering (GIWAXS) was also performed on these samples. Microscopy and spectroscopy measurements were accomplished at the 5.3.2.2 beamline of the Advanced Light Source at Lawrence Berkeley National Laboratory,[22,23] while those for scattering were conducted at the 7.3.3 beamline.[24] PSBTBT-08 was supplied by 1-Material with a Mw of 24 kg/mol and PDI of 2.1. PC61BM and PC71BM were supplied by Nano-C.

Microscopy images acquired of the various annealed blend films are displayed in Figure 2, which show micrometer-scale fullerene crystals that phase separate out of the blend over time. In the images, dark regions are fullerene crystals and light regions are the residual fullerene-depleted film as confirmed by NEXAFS spectra from each feature. The purity of the crystals is difficult to measure due to their large thickness, but no intermixing could be detected in the spectra. The blend with PC$_{61}$BM is shown in Figures 2a,b where different regions of the same film are imaged with a visible light microscope (VLM) and a scanning transmission X-ray microscope (STXM), respectively. In this case, annealing for 25 h was adequate for the initial (1:3) weight ratio blend to come to equilibrium, as can be seen by the lack of fullerene composition gradients measured in STXM. The composition in the regions between the crystals is thus a thermodynamic equilibrium composition in the presence of the fullerene crystals, which is naturally the result from a competition between the free energy of crystallization and the free energy of mixing. Notable in Figure 2a,b, two different PC$_{61}$BM crystal morphologies can be seen in the micrographs: one exhibiting a cubic-like appearance ∼1 μm in size and the other a much larger spatial extend, exhibiting a more typical elongated, branched morphology as seen when blended with P3HT.[25] These two crystal species have obviously different nucleation and growth mechanisms. Previous work on PC$_{61}$BM crystal formation suggested that the former species nucleate from the interface with the substrate where the fullerene tends to form a wetting layer during casting.[26] This species nucleates immediately upon annealing, consuming the fullerene surrounding it. In contrast, the species with cubic appearance nucleates later but is likely formed intrinsically within the bulk, suggesting that the initial blend ratio is inside the unstable region of the binary phase diagram. The C$_{70}$-based blends behave differently than those with PC$_{61}$BM, where PC$_{71}$BM show only one identifiable fullerene crystal species. The crystals are spaced further apart, taking longer to come to equilibrium (Figure 2c,d). After 25 h, PC$_{71}$BM depletion fronts can still be seen in the VLM image of Figure 2c and disappear with further annealing (Figure 2d), indicating that thermodynamic equilibrium has been attained. The lower nucleation density of the C$_{70}$-based fullerene crystals within the bulk could be advantageous for the stability of the morphology in devices, leading to longer device lifetimes. An important result from both systems is the lack of any fullerene-rich phase in which there is a partial miscibility of the polymer—only a polymer-rich phase was identified to the spatial limit of the STXM (∼30 nm).

GIWAXS patterns of the same polymer:fullerene blend films investigated for equilibrium composition are displayed in Figure 3 along with the pattern of a pure PC$_{71}$BM reference film. It is clear that after extended annealing the fullerene crystallizes very well with or without the polymer present. Of note is that the
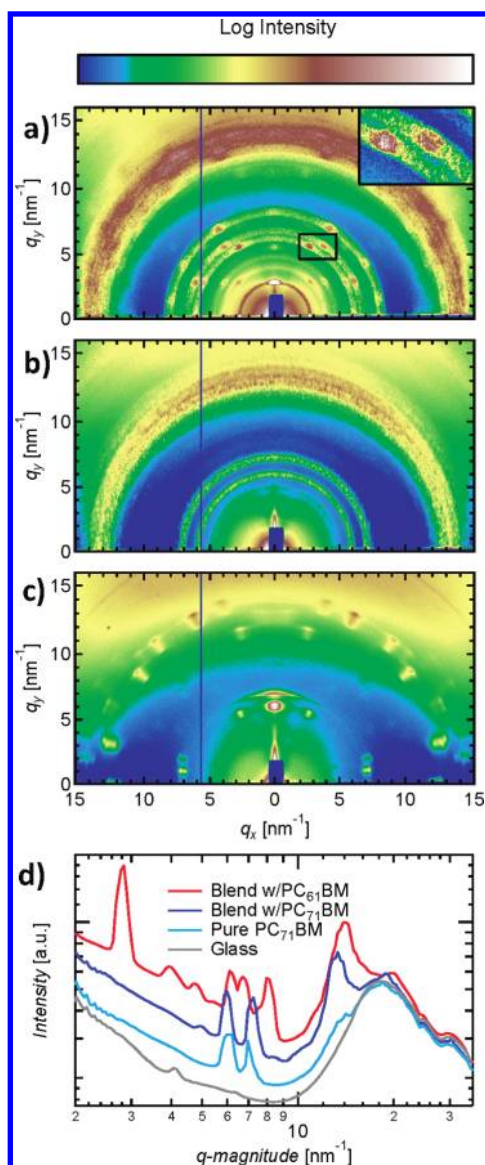
Figure 3. GIWAXS data and profiles from the same films investigated for miscibility: (a) raw data from the PSBTBT-08 blend with $PC_{61}BM$, (b) raw data from the PSBTBT-08 blend with $PC_{71}BM$, (c) raw data from a pure $PC_{71}BM$ film, and (d) circularly averaged scattering profiles.

Figure 4. Fits of NEXAFS acquired in fullerene-depleted regions of blend films brought to thermodynamic equilibrium: (a) PSBTBT:$PC_{71}BM$ and (b) PSBTBT:$PC_{61}BM$. Yellow and blue curves are from reference polymer and fullerene, respectively, and are plotted on an independent y-axis for comparison. Absorption data at the edge is expanded in energy for clarity.

scattering pattern from PSBTBT-08:$PC_{61}BM$ measured here (Figure 3a) is much richer than has been observed to date, exhibiting numerous highly textured reflections including an intense fundamental peak at 2.81 nm^{-1} corresponding to a spacing of 2.24 nm. To our knowledge, this reflection, has not yet been reported for GIWAXS; only the reflection at 14.0 nm^{-1} is typically observed in OPVs.[25] Such a large crystal spacing might occur if the side group on the fullerene exists in its trans-conformation as depicted in a recent report.[27] Remarkably, the GIWAXS and electron diffraction community has not yet converged on the precise crystal structure of $PC_{61}BM$ and $PC_{71}BM$;[27−29] however, a detailed crystallographic analysis is beyond the scope of this work. Because of the symmetry of the texture pattern all the diffraction features can be deduced to originate from the same crystal species including the low-q reflection (Figure S3), and therefore all features are associated with the
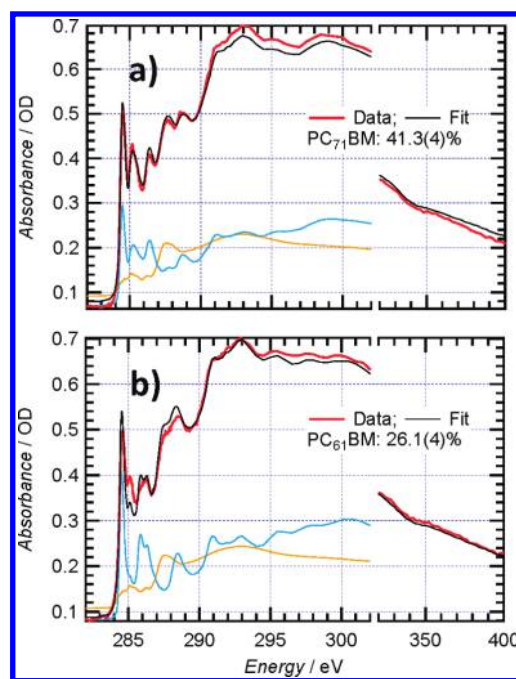
$PC_{61}BM$ crystallites as confirmed by GIWAXS on pure $PC_{61}BM$ films (Figure S4). Further evidence of this interpretation can be observed within each sample-broadened diffraction ring where isolated reflections from the individual nanocrystals result in individual small peaks that give rise to a speckled diffraction ring superimposed on the textured pattern (see Figure 3a inset). A Scherrer analysis on these individual speckle-like peaks is consistent with the size of the cube-like crystals seen in the STXM image (Figure 2b). Also of note is the richness and texture of the reflections in the $PC_{71}BM$ film in Figure 3c. Finally, the circularly averaged scattering profiles for each sample along with a bare glass substrate are displayed in Figure 3d. We do not detect any diffraction features previously observed for PSBTBT derivatives with different side chains such as diffraction peaks at $q = 4.04$ nm^{-1},[21] $q = 18.8$ nm^{-1},[17] or a lamellar spacing of 1.95 nm as seen in fiber X-ray scattering of PSBTBT-08.[18] Additionally, no diffraction was detected on pure films of PSBTBT-08 (Figure S2). All diffraction peaks in the blend films can be identified as those of the fullerenes. The GIWAXS thus demonstrates minimal if not a complete lack of crystallization of the PSBTBT-08 polymer, which is corroborated by the lack of the low-energy peak in the polymer's UV−vis spectrum (Figure S1) and its similarity to solution phase spectra.[18] Thus, crystallization of the PSBTBT-08 will not influence the miscibility measurements presented here, and the measured values can be used and interpreted without correction.

To measure the thermodynamic miscibility of each fullerene in PSBTBT-08, NEXAFS spectra of the residual polymer-rich regions in each film were acquired with a STXM[30,31] while avoiding the fullerene crystals. These spectra were then fit with reference spectra acquired from the pure components. An example of

typical fit results from multiple measurements and annealing times are displayed in Figure 4 and demonstrate the high quality of fits achieved using only two parameters (total thickness and relative composition). Since no polymer crystallization and preferential crystallite orientation (edge-on or face-on) was observed with GIWAXS, a polarization-dependent NEXAFS spectral factor that encodes preferential orientation[8] was not required in the fits for the PSBTBT-based blends. The fit of the blend with $PC_{71}BM$ in Figure 4a reproduces data very well while the fits for the $PC_{61}BM$-based blends are slightly worse, potentially due to preferential orientation of the polymer affecting the peak at 285.4 eV. However, this has only degraded the accuracy of the measurement slightly as the overall fit makes use of the large spectral differences across the full energy range. The resulting miscibility at 140 °C of the fullerenes with PSBTBT-08 extracted from multiple measurements of different films are 26(2) wt % and 41.1(5) wt % for $PC_{61}BM$ and $PC_{71}BM$, respectively. This is significantly higher than the fullerene miscibility in P3HT or MDMO-PPV previously measured. Additionally, it is of note that the miscibility of $PC_{71}BM$ is ∼60% higher by weight in the same polymer than that of $PC_{61}BM$. Combined with the previous results, this finding represents robust evidence that polymer–fullerene miscibility is potentially a universal property.

PSBTBT-08 was also used in blends with $PC_{71}BM$ to make devices, using the thermal annealing methodology reported previously[19] and the use of a solvent additive reported separately.[17] Of note is that these two reports use a polymer with the same backbone but differing side chains from the PSBTBT-08 used here. More information on the PSBTBT-08 polymer properties can be found in the Supporting Information, but the difference in side chains in the latter case involves a longer chain (dodecyl versus octyl) while the former is a shorter branched (2-ethylhexyl) side chain. The resulting device properties were poor irrespective of the fabrication method used, with power conversion efficiencies on the order of 0.1% or less with S-shaped $J–V$ curves, low external quantum efficiencies at both low and high photon intensities, and a 7-fold increase in photocurrent from short circuit to −1.0 V. The low performance of our PSBTBT-08:$PC_{71}BM$ blends, consistent with strong geminate recombination and an imbalance of charge mobilities, could be due to different sides chains of PSBTBT-08 used here. Transistor and X-ray diffraction studies by Beaujuge et al. on the same polymer as used here revealed low FET hole mobilities and an absence of π-stacking in neat films.[18] Specific processing parameters, $J–V$ data, and EQEs for each processing method can be found in the Supporting Information.

The result of a high miscibility in an amorphous polymer has significant implications for the operation and optimization of OPV devices beyond the universal phenomenon of fullerene miscibility in conjugated polymers. One important question that is raised by the existence of polymer–fullerene miscibility is to what extent amorphous regions help or hinder exciton dissociation, charge separation, and charge transport in an OPV device. High EQEs in the P3HT system[32] along with high $PC_{61}BM$ miscibility of ∼20 wt % we measured previously[8] suggest that molecular miscibility may be key to exciton dissociation and that charge transport can occur in the absence of pure phase separations via molecular percolation pathways so long as the miscibility is high enough to create molecular connectivity within the mixed phase. The high fullerene miscibility of more than 40 wt % as measured in the PSBTBT-08:$PC_{71}BM$ system here should easily cross such a molecular percolation threshold, yet device

performance suggests strong geminate recombination. Coupled with the lack of polymer crystallization seen in the annealed films, we hypothesize that high miscibility of the two materials alone is not enough to achieve good device performance, especially with potentially poor hole mobility[18] (i.e., molecular percolation can only separate and transport charge efficiently through a short length scale relative to the active layer thickness). Instead, other phases of either a network of crystallites (seen in P3HT) or a pure fullerene phase (seen with MDMO-PPV) is required to effectively transport the charge out of the device. Indeed, both PSBTBT device/morphology studies mentioned above which contain longer, shorter, and branched side chains exhibited a crystalline polymer phase.[17,19,21] Thus, the structure of the side chain is clearly an important factor in determining the crystallinity and morphology of the device and therefore the device characteristics. Lack of crystallinity through alteration of the side chain could also be the cause of poor mobilities measured in OTFT devices[18] due to poor interchain interactions. Consequently, careful design of backbone and side chains in semiconducting polymers should go beyond considerations of energy levels and common solubility with methanofullerenes.[33] It seems reasonable that the miscibility measured in this polymer be similar to that in amorphous portions of others with the same backbone, since the interaction is often dominated between aromatic groups of the two materials.[34] In the case of the acceptor, it is also important to note the significant difference of molecular miscibility shown here as a function of fullerene species. Past and ongoing studies of different fullerene moieties typically focus on optimizing the electronic properties of the material with mixed results in actual devices.[35−38] The results presented here demonstrate the need to also consider the high variability of molecular miscibility with the polymer, potentially important to device performance. In addition to showing that polymer–fullerene miscibility is likely universal, this work clearly reveals the need for a better understanding of how a polymer's side chain affects blend crystallinity and morphology and how this, in concert with fullerene miscibility in the amorphous regions, determines the device performance.

■ EXPERIMENTAL METHODS

Sample Preparation for Films at Thermodynamic Equilibrium. Blend films were cast from solutions of (1:3) polymer/fullerene by weight, 40 g/L in chlorobenzene at various spin speeds for thickness variation onto NaPSS-coated cleaned glass slides. A pure film of PSBTBT was cast from a 30 g/L chlorobenzene solution. For NEXAFS spectral measurement of the fullerenes, films were drop-cast from 2 g/L chlorobenzene solutions onto SiN windows. All solutions were stirred and heated to 40 °C overnight to allow for the materials to be completely dissolved. Once cast, a set of films were annealed at 140 ± 5 °C on a covered hot plate in a glovebox under 1 ppm of O_2 and H_2O nitrogen environment for either 25 or 116 h. The temperature was measured via a NIST-calibrated surface thermometer within the sample chamber. Pieces of the films (a few millimeters) were floated off the substrate by dissolving the NaPSS layer in deionized water and were picked up on Cu TEM grids for investigation in the STXM. The rest of the film was used for the GIWAXS study.

Grazing Incidence Wide-Angle Scattering (GIWAXS). The blend films that were studied for phase composition (annealed for 116 h) were investigated via GIWAXS at the 7.3.3 beamline of the Advanced Light Source. The 10 keV beam was incident on the samples at 0.08°, 0.12°, and 0.16°. Very little differences in scattering patterns were found as the samples were very rough and scattering from the glass substrate could be seen, indicating a bulk measurement at all angles. Therefore,

scattering at the angle with the fewest parasitic scattering effects (0.08°) was used for the figures displayed here. The scattered intensity was collected by an ADSC Quantum 4 CCD. A plastic bag with helium flow surrounded the entire photon path to minimize air scatter. The $PC_{71}BM$ film was cast from 50 g/L chlorobenzene solutions onto an NaPSS-coated glass slide and was annealed to crystallize the fullerene.

■ ASSOCIATED CONTENT

ⓢ Supporting Information. Material information and solid state UV—vis spectrum; PSBTBT-08:$PC_{71}BM$ device processing and testing description and results. This material is available free of charge via the Internet at http://pubs.acs.org.

■ ACKNOWLEDGMENT

■ REFERENCES

(1) Brabec, C. J.; Gowrisanker, S.; Halls, J. J. M.; Laird, D.; Jia, S.; Williams, S. P. *Adv. Mater.* **2010**, *22*, 3839.

(2) Blom, P. W. M.; Mihailetchi, V. D.; Koster, L. J. A.; Markov, D. E. *Adv. Mater.* **2007**, *19*, 1551.

(3) Yan, H.; Swaraj, S.; Wang, C.; Hwang, I.; Greenham, N. C.; Groves, C.; Ade, H.; McNeill, C. R. *Adv. Funct. Mater.* **2010**, *20*, 4329.

(4) Aarnio, H.; Sehati, P.; Braun, S.; Nyman, M.; de Jong, M. P.; Fahlman, M.; Österbacka, R. *Adv. Energy Mater.* **2011**.

(5) Watkins, P. K.; Walker, A. B.; Verschoor, G. L. B. *Nano Lett.* **2005**, *5*, 1814.

(6) Chen, L.-M.; Hong, Z.; Li, G.; Yang, Y. *Adv. Mater.* **2009**, *21*, 1434.

(7) Watts, B.; Belcher, W. J.; Thomsen, L.; Ade, H.; Dastoor, P. C. *Macromolecules* **2009**, *42*, 8392.

(8) Collins, B. A.; Gann, E.; Guignard, L.; He, X.; McNeill, C. R.; Ade, H. *J. Phys. Chem. Lett.* **2010**, *1*, 3160.

(9) Kiel, J. W.; Eberle, A. P. R.; Mackay, M. E. *Phys. Rev. Lett.* **2010**, *105*, 168701.

(10) Chen, D.; Nakahara, A.; Wei, D.; Nordlund, D.; Russell, T. P. *Nano Lett.* **2010**, *11*, 561.

(11) Treat, N. D.; Brady, M. A.; Smith, G.; Toney, M. F.; Kramer, E. J.; Hawker, C. J.; Chabinyc, M. L. *Adv. Energy Mater.* **2011**, *1*, 82.

(12) Yin, W.; Dadmun, M. *ACS Nano* **2011**, *5*, 4756.

(13) Chen, D.; Liu, F.; Wang, C.; Nakahara, A.; Russell, T. P. *Nano Lett.* **2011**, *11*, 2071.

(14) Cates, N. C.; Gysel, R.; Beiley, Z.; Miller, C. E.; Toney, M. F.; Heeney, M.; McCulloch, I.; McGehee, M. D. *Nano Lett.* **2009**, *9*, 4153.

(15) Price, S. C.; Stuart, A. C.; Yang, L.; Zhou, H.; You, W. *J. Am. Chem. Soc.* **2011**, *133*, 4625.

(16) Huo, L.; Guo, X.; Zhang, S.; Li, Y.; Hou, J. *Macromolecules* **2011**, *44*, 4035.

(17) Coffin, R. C.; Peet, J.; Rogers, J.; Bazan, G. C. *Nature Chem.* **2009**, *1*, 657.

(18) Beaujuge, P. M.; Pisula, W.; Tsao, H. N.; Ellinger, S.; Müllen, K.; Reynolds, J. R. *J. Am. Chem. Soc.* **2009**, *131*, 7514.

(19) Hou, J.; Chen, H.-Y.; Zhang, S.; Li, G.; Yang, Y. *J. Am. Chem. Soc.* **2008**, *130*, 16144.

(20) Wang, E.; Wang, L.; Lan, L.; Luo, C.; Zhuang, W.; Peng, J.; Cao, Y. *Appl. Phys. Lett.* **2008**, *92*, 033307.

(21) Chen, H.-Y.; Hou, J.; Hayden, A. E.; Yang, H.; Houk, K. N.; Yang, Y. *Adv. Mater.* **2010**, *22*, 371.

(22) Warwick, T.; Ade, H.; Kilcoyne, A. L. D.; Kritscher, M.; Tylisczcak, T.; Fakra, S.; Hitchcock, P.; Hitchcock, A. P.; Padmore, H. A. *J. Synchrotron Radiat.* **2002**, *9*, 254.

(23) Kilcoyne, A. L. D.; Tyliszczak, T.; Steele, W. F.; Fakra, S.; Hitchcock, P.; Franck, K.; Anderson, E.; Harteneck, B.; Rightor, E. G.; Mitchell, G. E.; Hitchcock, A. P.; Yang, L.; Warwick, T.; Ade, H. *J. Synchrotron Radiat.* **2003**, *10*, 125.

(24) Hexemer, A.; et al. *J. Phys.: Conf. Ser.* **2010**, *247*, 012007.

(25) Woo, C. H.; Thompson, B. C.; Kim, B. J.; Toney, M. F.; Fréchet, J. M. J. *J. Am. Chem. Soc.* **2008**, *130*, 16324.

(26) He, C.; Germack, D. S.; Joseph Kline, R.; Delongchamp, D. M.; Fischer, D. A.; Snyder, C. R.; Toney, M. F.; Kushmerick, J. G.; Richter, L. J. *Sol. Energy Mater. Sol. Cells* **2011**, *95*, 1375.

(27) Bazylewski, P. F.; Kim, K. H.; Forrest, J. L.; Tada, H.; Choi, D. H.; Chang, G. S. *Chem. Phys. Lett.* **2011**, *508*, 90.

(28) Sanyal, M.; Schmidt-Hansberg, B.; Klein, M. F. G.; Munuera, C.; Vorobiev, A.; Colsmann, A.; Scharfer, P.; Lemmer, U.; Schabel, W.; Dosch, H.; Barrena, E. *Macromolecules* **2011**, *44*, 3795.

(29) Verploegen, E.; Mondal, R.; Bettinger, C. J.; Sok, S.; Toney, M. F.; Bao, Z. *Adv. Funct. Mater.* **2010**, *20*, 3519.

(30) Ade, H.; Zhang, X.; Cameron, S.; Costello, C.; Kirz, J.; Williams, S. *Science* **1992**, *258*, 972.

(31) Ade, H.; Stoll, H. *Nature Mater.* **2009**, *8*, 281.

(32) Schilinsky, P.; Waldauf, C.; Brabec, C. J. *Appl. Phys. Lett.* **2002**, *81*, 3885.

(33) Liang, Y.; Feng, D.; Wu, Y.; Tsai, S.-T.; Li, G.; Ray, C.; Yu, L. *J. Am. Chem. Soc.* **2009**, *131*, 7792.

(34) Yang, C.; Hu, J. G.; Heeger, A. J. *J. Am. Chem. Soc.* **2006**, *128*, 12007.

(35) Zhao, G.; He, Y.; Li, Y. *Adv. Mater.* **2010**.

(36) Troshin, P. A.; Hoppe, H.; Renz, J.; Egginger, M.; Mayorova, J. Y.; Goryachev, A. E.; Peregudov, A. S.; Lyubovskaya, R. N.; Gobsch, G.; Sariciftci, N. S.; Razumov, V. F. *Adv. Funct. Mater.* **2009**, *19*, 779.

(37) He, Y.; Zhao, G.; Peng, B.; Li, Y. *Adv. Funct. Mater.* **2010**, *20*, 3383.

(38) Mikroyannidis, J. A.; Kabanakis, A. N.; Sharma, S. S.; Sharma, G. D. *Adv. Funct. Mater.* **2011**, *21*, 746.